Shielded Cable Transfer Impedance Measurements High frequency range 100 MHz–1 GHz

B. Démoulin, L. Koné
TELICE-IEMN Group, Université Lille 1, (France)

Introduction

In our previous paper [1] we described the setup for the measurement of the transfer impedance of shielded coaxial cables. We demonstrated that the conventional triaxial setup does not allow to reach frequencies higher than 100 MHz, mainly due to the onset of propagation phenomena. In fact, for a cable sample of 1 m in length, the maximum frequency attainable by means of a measurement of the near-end crosstalk voltage does not exceed 30 MHz. On the other hand, if we measure the far-end crosstalk voltage, the maximum attainable frequency can grow up to 100 MHz. However, the technology of the transfer impedance bench setup must be modified, in order to be able to explore the bandwidth between 100 MHz and 1 GHz.

It is a known fact that the accuracy produced by a purely computational compensation of propagation phenomena is not acceptable; hence, a more rational approach to the reduction of the propagation effects is the reduction of the physical length of the sample under test. The rule of proportionality with wavelength teaches us that we need to reduce the dimension by a factor of

10 (i.e., adopt samples of 10 cm), in order to reliably measure up to 1 GHz, without being affected by propagation. On the other hand, at higher frequencies, mismatches of the perturbation line tend to amplify, especially at the line extremities where the signal source and the matched load are connected. The consequence of such defects is to produce an uncertain estimate of the perturbation current, which–in turn–results in a non-negligible error of the transfer impedance estimate. All the above reasons call for an adjustment of the technology of the transfer impedance bench setup to the extension of the frequency range [2], [3].

The first Section of this article concerns the description of two transfer impedance setups, whose configurations have been devised in particular for reducing the mismatch defects for cable samples of 10 cm in length. We first describe the wire injection method, the construction principle of which resides in a perturbation line made by a thin ribbon conductor glued on the cable insulating jacket. Then we introduce the shield discontinuity method, by which the sample under test represents the inner conductor of a coaxial cavity terminated by a short circuit. The second Section deals with the calibration of the above setups by

means of samples made by a coaxial homogeneous tube with one or more apertures. We will compute the transfer inductance of these samples with the aim of determining their transfer impedance in the frequency range 100 MHz–1 GHz. The third Section presents measurement results obtained for a calibration sample with one aperture, and for a 10-cm long cable with a braided shield.

Improvement of the Measurement Setups for High Frequency Range

Ignoring propagation phenomena, the transfer impedance is generally directly proportional to the ratio between the measured voltage V_{cM} at the end of the sample under test and the current I_m, injected into the cable shield with length L_0, i.e.,

$$Z_{tM} = \frac{2}{L_0} \frac{V_{cM}}{I_m} \tag{1}$$

Since, as we mentioned, several imperfections introduced by the injection current measurement are due to propagation phenomena, we can easily correct them using expressions found in [1] which include the contribution of the propagation phenomena. Theoretically, the transfer impedance Z_t can be obtained by means of the following expression, if the near-end crosstalk voltage is used in (1),

$$Z_t = \frac{Z_{tM}}{F_0(\omega, L_0)} \tag{2}$$

while an alternate expression for the transfer impedance Z_t is needed, if far-end crosstalk voltage measurements are employed:

$$Z_t = \frac{Z_{tM}}{F_{L_0}(\omega, L_0)} \tag{3}$$

In practice, these corrections are only usable for frequencies situated below the first zero of the denominator functions in (2) and (3). The functions $F_0(\omega, L_0)$ and $F_{L_0}(\omega, L_0)$ as appearing at denominators in equations (2) and (3) are developed in [1], these fall to zero at the following frequencies f_n and f_p :

$$F_0(\omega_n, L_0) = 0 \quad \rightarrow \quad f_n = \frac{n}{\left(\frac{1}{v_1} + \frac{1}{v_2}\right) L_0} \tag{4}$$

$$F_{L_0}(\omega_p, L_0) = 0 \quad \rightarrow \quad f_p = \frac{p}{\left|\frac{1}{v_1} - \frac{1}{v_2}\right| L_0} \tag{5}$$

We can notice in these formulas that the parameters v_1 and v_2 correspond to the speeds of the currents and voltages in the disturbing line and the coaxial cable respectively.

As an example, let us consider a triaxial setup, the length of which is $L_0 = 1$ m and the propagation velocities compared to the speed of light are $v_1 = 0.8\ c$, and $v_2 = 0.6\ c$. The first ($n = 1$) near-end voltage zero appears at $f_1 = 102$ MHz, and the first ($p = 1$) far-end voltage zero at $f_1 = 720$ MHz. Since the measured voltage "minimum" is not exactly a "zero" (as predicted by (4) and (5)), the correction in proximity of these frequencies will be affected by a significant error.

This method is therefore not really usable in this example for frequencies lower than 50 MHz; however, the limit of this correction can be extended to 300 MHz if we use far-end voltage.

To obtain measurements usable up to 1 GHz, it is essential to reduce the dimensions L_0 of the sample, in order to avoid high-frequency propagation phenomena. Thus, a 10-cm test sample brings the near-end voltage limit to 500 MHz, and to 3 GHz for far-end voltage. However, it should be mentioned that the previously-described triaxial setup is not recommended for samples of small dimensions. Moreover, leakage localized at sample cable terminations leads to additional errors (some specific arrangements involved by use of sample with 10 cm small dimension was necessary for reaching reliable measurements). The following is dedicated to the description of measurement setups with the so called wire injection and shield discontinuity methods, that are more suitable for high frequencies than classical triaxial arrangements.

Measurement Setup with Wire Injection Method

Fig. 1 shows the longitudinal section of an impedance measurements bench based on the wire injection method.

The perturbing line consists of a conductor of length L_0 tied to the external insulating sheath of the cable under test. Fig. 2 represents a transverse section localized in the median part of the measurement device. The width of the self-sticky metallic
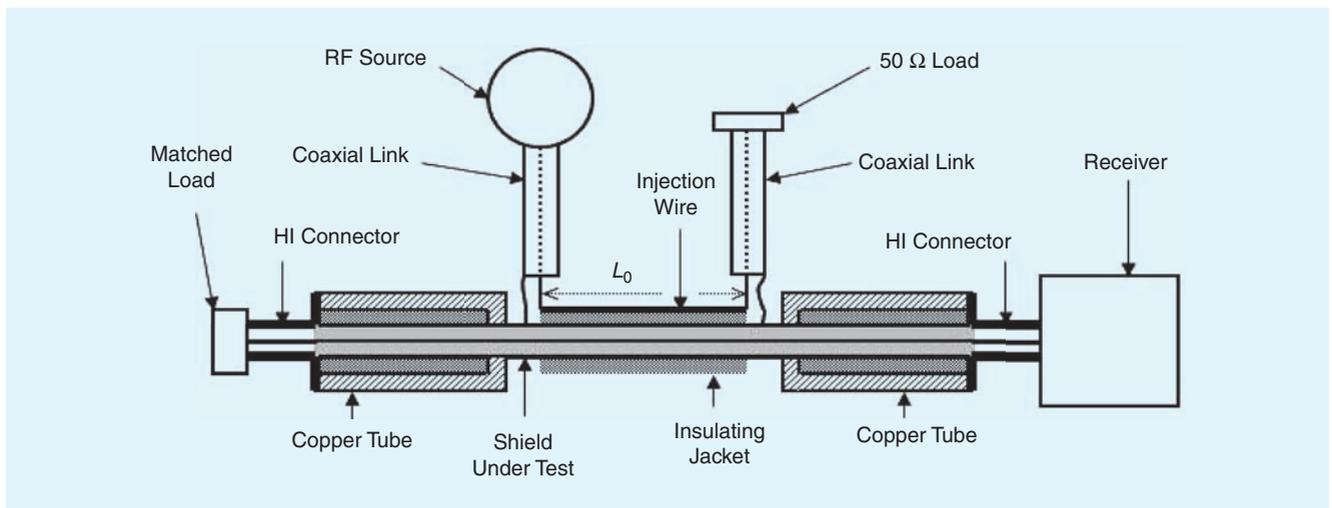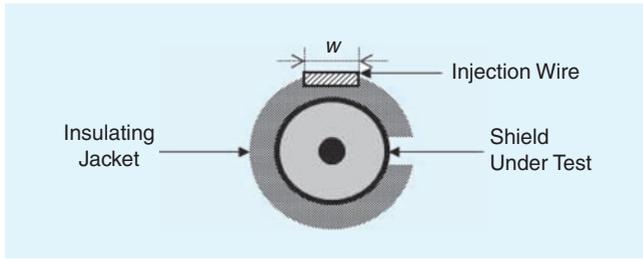

Fig. 1. Description of the wire injection setup.

Fig. 2. View of the cross section of the cable under test showing the location of the injection wire.

strap is determined so that the characteristic impedance of the relevant transmission line is 50 Ω. A high-frequency source is connected to this input line through a coaxial cable of characteristic impedance 50 Ω.

A second coaxial connection, symmetrical to the previous one, connects the line extremity with the 50 Ω matched impedance.

Like in the classic triaxial setup, the injection wire connected with the source voltage produces an electromagnetic radiation in proximity of the measurements bench. It is therefore essential to protect the passive terminations of the sample with additional shielding. This involves homogeneous copper (or tin) pipes providing a uniform electric contact with the shield periphery, situated at the ends of the perturbed zone. Far-end voltage is measured by means of a spectrum analyser connected to the end of the cable under test, opposite to the injection point; the other end of the cable is terminated on a matched load.
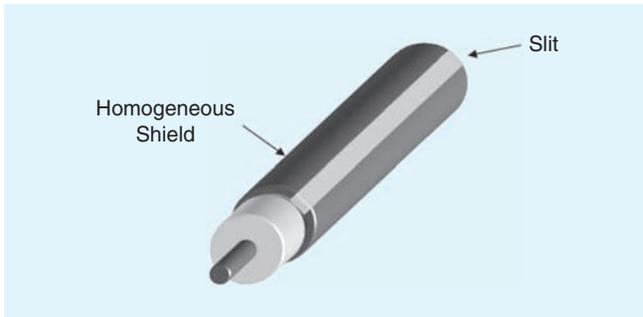

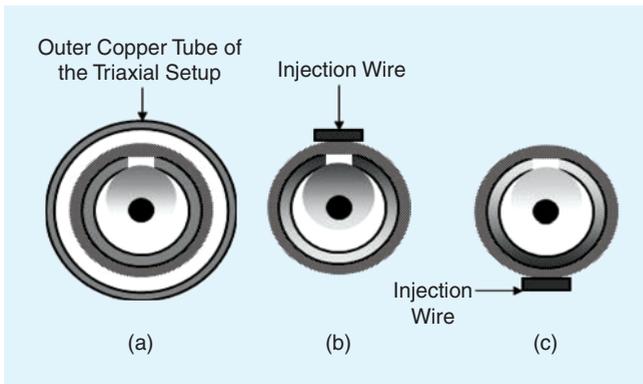
Fig. 3. Cable shield configuration with a slit.

Fig. 4. Various conditions of the magnetic field leakage depending of the current density distribution throughout the cable shield cross section. (a) Current density with uniform distribution. (b) Current density increased near the location of the shield slit. (c) Current density increased at the opposite side of the shield slit.

This measurement technique allows for the continuous exploration of frequencies from about 1 kHz to 1 or 2 GHz. As pointed out above, the sensitivity of this method is limited by the wire radiation, and in order to reach transfer impedance values below 100 $\mu\Omega$/m we need to adopt the special precautions described in reference [1].

Contrary to the triaxial setup, the current distribution in the transverse section of the shield under test is not exactly uniform. Therefore, the measured transfer impedance will depend on the angular position of the wire. This phenomenon is particularly visible when the shield structure departs from a perfectly cylindrical shape. For instance, Fig. 3 shows a homogeneous shield with a defective coverage, constituted by a slit placed on the cylinder generatrix.

Fig. 4 shows the current density throughout the cross section of the sample either for: **(a)** a uniform distribution in the triaxial setup, or for **(b)** a nonuniform variation realized by means of the injection wire placed in front of the slit, or **(c)** opposed to it. The shadowed circles under the slit indicate the relative intensity of the magnetic field leakage, which, of course, reaches its maximum in the disposition **(b)** and has its minimum in disposition **(c)**. Consequently, we appreciate that the test performed with the triaxial setup reproduces a global transfer impedance, that can be found in this second method by means of an average of the measurements realized placing the coupling wire at four test points of the cross-section separated by 90 degrees.

Triaxial Setup with Shield Discontinuity Method

This technique uses resonance properties of a triaxial setup constituted by a short-circuited perturbing line; Fig. 5 shows a longitudinal cross-section of such setup.

The sample cable is placed inside metallic pipes which create the central conductor of a coaxial cavity; such pipes also have a complementary shielding function. In fact, the sample is interrupted in the middle for a short distance L_0 that represents a "discontinuity". With this procedure, we partially expose the shielded cable under test to the perturbing current produced by a high-frequency source connected at the cavity input. The equivalent circuit shown in Fig. 6 helps in describing the measurement setup working principle.

The perturbing line, short-circuited at one end, is therefore powered by the high frequency voltage source E_0 with internal impedance Z_0, generating a current distribution $I_1(z)$ and a voltage distribution $V_1(z)$. The hatched region indicates the part of the shield really exposed to the perturbing current indicated in
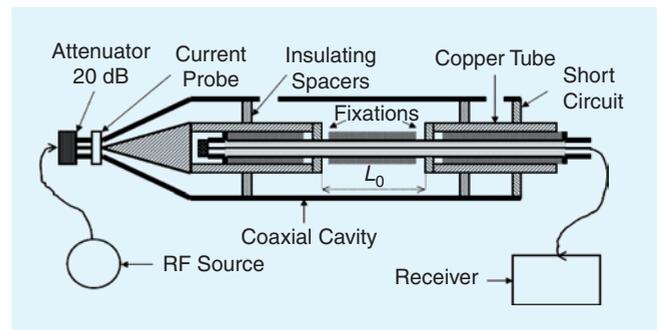

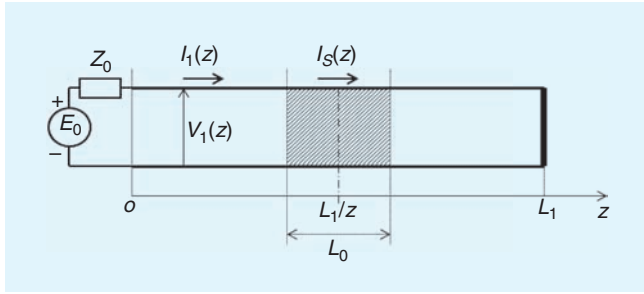*Fig. 5. Description of the setup named shield discontinuity method.*

Fig. 6. Transmission line arrangement for the computation of the current $I_S(z)$ at the shield discontinuity.

this point by $I_S(z)$. The discontinuity is preferably placed in the median part of the line (i.e., at $z = L_1/2$), where the parameter L_1 represents the cavity longitudinal dimension.

The transverse dimension of the perturbing line is chosen to produce a characteristic impedance Z_{c1} close to 50 Ω, and the spacers have a slight influence on the electromagnetic field configuration. We assume that the propagation constant γ_1 in the cavity is close to the value in air, that is:

$$\gamma_1 = jk \cong j\frac{\omega}{c} \tag{6}$$

An additional simplification assumes that the geometrical transition at the discontinuity does not modify the local characteristic impedance. Under the above hypotheses, a simple analytical expression for $I_1(z)$ is derived:

$$I_1(z) = I_0\cos[k(L_1 - z)] \tag{7}$$

where the amplitude I_0 becomes

$$I_0 = \frac{E_0}{Z_0\cos(kL_1) + jZ_{c1}\sin(kL_1)} \tag{8}$$

The measurement principle exploits the current behaviour $I_S(z)$ observed at the cavity resonance. The following numerical example should clarify these phenomena. A coaxial cavity has a longitudinal dimension $L_1 = 70$ cm and a characteristic impedance $Z_{c1} = 50$ Ω; the propagation velocity of the TEM mode is $v_1 = c$. The source can be connected to the line in two different configurations:
1) Matched source (without attenuator) with voltage amplitude $E_0 = 10$ V and impedance $Z_0 = Z_{c1} = 50$ Ω
2) Sources with a 20 dB attenuator and voltage amplitude $E_0 = 1$ V and impedance $Z_0 = Z_{c1} = 5$ Ω

Fig. 7 shows the current computed in the median part of the cavity $I_1(L_1/2)$ as a function of frequency. The thin line represents the simulation obtained with the matched source, while the thick line refers to the current with the insertion of a 20 dB attenuator between matched source and cavity input.

This theoretical result suggests that the current graph can be subdivided into three different regions. The low frequencies region spreads from 10 kHz to 30 MHz; here, the transfer impedance can be directly determined by the ratio between the voltage collected at the end of the sample and the current measured at the cavity input. The middle frequencies region covers in this example the range between 30 MHz and 150 MHz: here, the correct evaluation of the transfer impedance needs a mathematical correction. The high frequencies region, situated between 150 MHz and 3 GHz, allows the direct measurement of
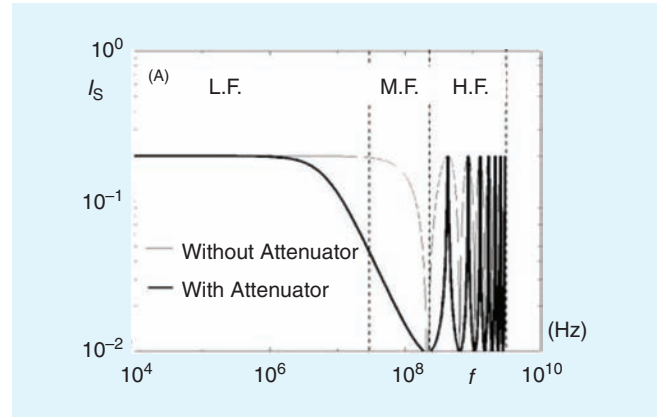

Fig. 7. Variations vs the frequency of the current $I_S(z)$ with and without attenuator inserted between the RF Source and the input port of the setup.
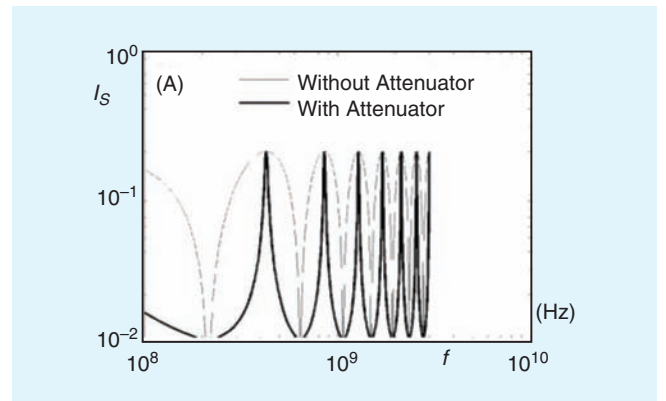

Fig. 8. Zoom about the resonances occurring on the current $I_S(z)$ at the shield discontinuity, these are lesser damped when the attenuator is inserted.

the transfer impedance: this is done at the particular frequencies imposed by longitudinal cavity resonances, i.e. for the specific frequencies f_n given by the following condition:

$$\cos\left(k\frac{L_1}{2}\right) = \pm 1 \quad \rightarrow \quad f_n = n\frac{c}{L_1} \tag{9}$$

For the example considered above, such frequencies assume the values of 428 MHz, 857 MHz, 1.3 GHz, 1.7 GHz, 2 GHz, 2.5 GHz, etc. Considering the cavity transverse dimensions (usually in the range of 7–8 cm), the exploitation of frequencies above 3 GHz is not advisable, due to the errors introduced by the excitation of TE and TM modes in the cavity.

A zoom of Fig. 8 between 100 MHz and 3 GHz shows details about resonance selectivity.

We can see that a matched source produces broad resonances because of the high damping of the circuit. We can reduce this phenomenon by reducing the source output impedance through the interposition of an attenuator, that also helps protecting the radio frequency generator from the overload produced by the wide range of impedance variations at the cavity input.

It can be shown that in the high frequencies region, the transfer impedance can be evaluated by the voltage-current ratio at the resonances, i.e.

$$|Z_t| \cong \frac{2}{L_0}\left|\frac{V_2(L_0)}{I_1(L_1/2)}\right|_{f=f_n} \tag{10}$$
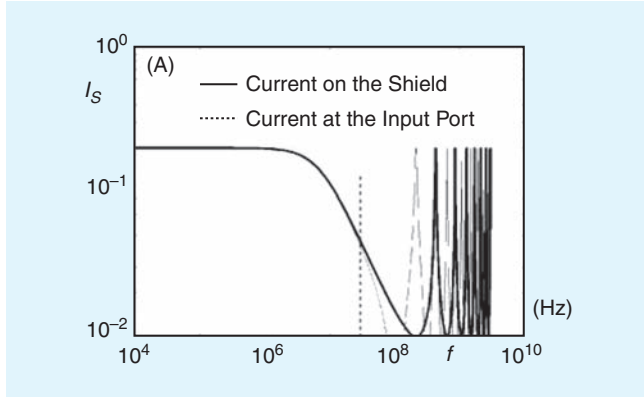
Fig. 9. The resonances are shifted in respect of the location of the current along the inner conductor of the coaxial cavity.
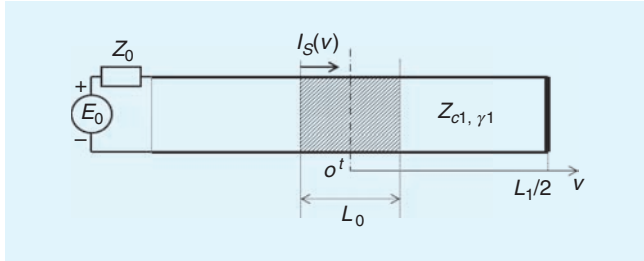

Fig. 10. Transmission line arrangement for the computation of the voltage at the end of the shielded cable under test.

Current $I_1(L_1/2)$ cannot be evaluated in the central part of the sample; hence, its indirect evaluation can be realized by means of a current sensor placed at the cavity input. For the previous example, the curves of Fig. 9 compare the currents computed at the median point and at the input of the sample.

For low frequencies between 10 kHz and 30 MHz, the two current values are identical, and a similar observation applies for resonance peaks at high frequencies. However, at intermediate frequencies between 30 MHz and 100 MHz, significant differences are observed and predictions require the application of a correction factor.

To evaluate the voltage $V_2(L_1)$, we can use the longitudinal coordinates shift shown in Fig. 10.

The new coordinate v is defined as

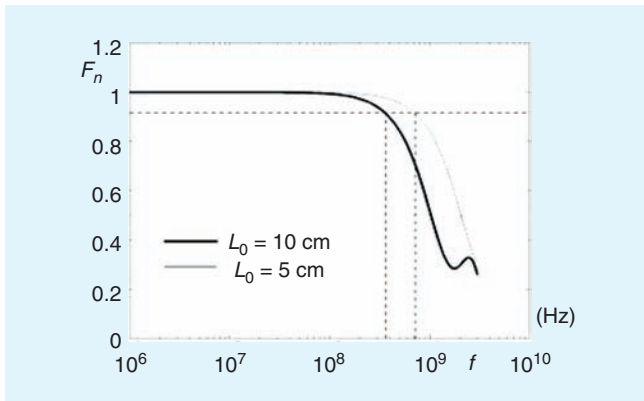$$v = z - \frac{L_1 - L_0}{2} \qquad (11)$$

Fig. 11. Change in shape of the function $F_n(\omega, L_0)$ with the length L_0 of the shield Discontinuity.

At resonance frequencies, the shield current $I_{Bn}(v)$ takes the expression:

$$I_{Sn}(v) = I_{0n}\cos(k_n v) \qquad (12)$$

where the current amplitude is virtually independent of the resonance order, i.e.

$$I_{0n} = \frac{E_0}{Z_0} \qquad (13)$$

The voltage generated at the sample end in presence of resonances is then expressed by the following integral:

$$V_2(L_1) = (-1)^n \frac{1}{2} Z_t I_{0n} e^{-\gamma_2 L_1/2} \int_{-L_0/2}^{L_0/2} ch(\gamma_1 v)\, e^{-\gamma_2 v} dv \qquad (14)$$

This integral produces a correction function $F_n(\omega_n, L_0)$ to be applied to the voltage determined at low frequencies:

$$V_2(L_1) = (-1)^n \frac{1}{2} Z_t I_{0n} L_0 F_n(\omega_n, L_0) \qquad (15)$$

where the factor $F_n(\omega_n, L_0)$ takes the following analytical form:

$$F_n(\omega_n, L_0) = \frac{1}{2} \frac{sh\left[(\gamma_1 + \gamma_2)\dfrac{L_0}{2}\right]}{(\gamma_1 + \gamma_2)\dfrac{L_0}{2}} e^{-\gamma_2 L_1/2}$$
$$+ \frac{1}{2} \frac{sh\left[(\gamma_1 - \gamma_2)\dfrac{L_0}{2}\right]}{(\gamma_1 - \gamma_2)\dfrac{L_0}{2}} e^{-\gamma_2 L_1/2} \qquad (16)$$

Using the previous numerical example, correction curves can be generated according to (16). The coaxial cavity is characterized by a length $L_1 = 70$ cm and a characteristic impedance $Z_{c1} = 50\ \Omega$; the TEM-mode propagation velocity on the perturbing line is $v_1 = c$ and inside the sample cable it amounts to $v_2 = 0.6c$. The curves of Fig. 11 show simulations results for two discontinuities with different dimensions, as follows: $L_0 = 10$ cm (the corresponding line is the thicker one) and $L_0 = 5$ cm (thinner line).

The intercepts of the curves in Fig. 11 with the 0.9 and 0.5 levels identify those frequencies for which the error introduced by propagation phenomena represents 10% or 50% of the low-frequency impedance value, respectively, as summarized in the following table.

The above errors can be compensated during the measurement by means of the calculation of function (16).

Since tubular shields placed on both parts of the discontinuity generally exceed the sample diameter, we can adjust the inaccuracy produced by the characteristic impedance transition by means of other expressions not given here.

$L_0 = 10$ cm	$\varepsilon = 10\%$	$\rightarrow$	$f = 400$ MHz
	$\varepsilon = 50\%$	$\rightarrow$	$f = 1$ GHz
$L_0 = 5$ cm	$\varepsilon = 10\%$	$\rightarrow$	$f = 700$ MHz
	$\varepsilon = 50\%$	$\rightarrow$	$f = 2$ GHz

Contrary to the coupling-wire setup previously described, the discontinuity method adopts a closed coaxial structure confining the electromagnetic energy around the sample under test. This configuration reduces the risk of parasitic coupling and allows a sensitivity improvement, attaining a level of $\mu\Omega$/m for frequencies up to hundreds of MHz. This measurement method is recommended for the qualification of high-immunity cables or shielded connectors.

Above 3 GHz, the methods discussed above generate significant errors due to the appearance oh higher-order propagation modes in the setup. An alternative approach consists in replacing the measurement of the transfer impedance with the determination of the shielding attenuation performed in a stirred-mode reverberation chamber.

Calibration Method for High Frequency Range

In our previous paper [1] we showed that the calibration of the measurement setup for the transfer impedance of shielded cables requires a specific sample made of a homogenous metal conductor in a form of a tube. In fact, the transfer impedance of such sample can be determined by the Schelkunoff's formula [1] which may be also found in the first term of equation (17) of this paper. The comparison of the measured value of the transfer impedance with the computed result was used in our previous work to point out to some imperfections of the measurement setup, in particular the effect of field leakage in the contact zone between the sample and the rest of the setup. Also, exploiting the fact that the transfer impedance of a homogeneous metallic tube monotonically decreases with the increasing frequency, we showed that the calibration sample allows to determine the measurements sensitivity, defined as the minimum measurable threshold, usually given by a multiple or submultiple of $\mu\Omega$/m.

Knowing that the transfer impedance of a copper tube, whose thickness is on the order of a tenth of a millimeter, attains values below 1 $\mu\Omega$/m at frequencies above 70 MHz, we cannot expect to use this sample to calibrate a measurement setup in the frequency range 100 MHz–1 GHz. In fact, the increase of frequency has the inevitable consequence of increasing the amplitude of induced voltages due to leakage, and the sensitivity in this frequency range surpasses the threshold of 1 $\mu\Omega$/m, attaining values towards 10 or 100 $\mu\Omega$/m. The use of homogeneous shields of thickness lower than 100 μm would allow to reach an acceptable threshold also in the frequency range 100 MHz–1 GHz, but experience has demonstrated that it becomes rather difficult to realise tight contacts at the sample extremities, thus making the calibration results too influenced by field leakage.

For the above reasons, at frequencies above 100 MHz, we adopt samples having their transfer impedance determined by the electromagnetic coupling produced by a small circular aperture. Fig.12 provides construction details of the this sample, which is represented by a piece of coaxial cable, whose longitudinal dimension is determined according to the previously defined criteria. The sample requires a homogenous copper shield of thickness E, whose suggested order of magnitude will be specified later on. The magnetic coupling is produced by a small circular aperture of diameter d through the shield surface [6].

The transfer impedance of such sample takes the following expression :

$$Z_t = R_0 \frac{(1+j)\dfrac{E}{\delta}}{sh\left[(1+j)\dfrac{E}{\delta}\right]} + j\,L_t\omega \qquad (17)$$

The first term of (17) represents the coupling due to the diffusion of the electric field tangential to the surface of the copper shield; in fact, this term contains the shield thickness E, its per-unit-length resistance R_0 and the skin depth δ. The second term $L_t\omega$ expresses the voltage induced by the electromagnetic coupling through the circular aperture; it contains the angular frequency ω of the sinusoidal perturbing current injected along the shield and the transfer inductance of the aperture L_t. We must realize that, in the frequency range between 100 MHz and 1 GHz, a hole of diameter d on the order of a millimeter and a copper tube of thickness E larger than 100 μm, give rise to a term $L_t\omega$ that is largely dominant in eq. (17), i.e.,

$$d \geq 1mm \quad \text{and} \quad E \geq 100\,\mu m \quad \rightarrow \quad Z_t \cong j\,L_t\omega \quad (18)$$

Consequently, the measured transfer impedance of this sample with a hole is proportional to the frequency; hence, the graph of the amplitude of Z_t is a straight line whose slope is determined by the value of L_t. Therefore, the superposition of the theoretical straight line depending on L_t and the measured transfer impedance allows us to evidence possible discrepancies, revealing calibration defects of the measurements setup.

The coupled line theory help us to show that the sample transfer inductance L_t depends on the diameter D of the shield, as follows:

$$L_t = \frac{\mu_0\,\alpha_m}{\pi^2\,D^2} \qquad (19)$$

where $\mu_0 = 4\pi 10^{-7}$ H/m is the magnetic permeability of vacuum and α_m is the coefficient of magnetic polarizability of the aperture [5], which, for a small circular hole, can be analytically determined by means of the plane-wave diffraction theory:

$$d \ll D \quad \text{and} \quad E \ll d \quad \rightarrow \quad \alpha_m = \frac{d^3}{6} \qquad (20)$$

It should be pointed out that the validity of the above (19) and (20) requires that the hole diameter d is much larger than the thickness E but much smaller than the shield diameter D.

By means of several samples with apertures of decreasing diameters, we can observe that the coefficient α_m–proportional to d^3–generates voltages of decreasing amplitudes at the end of the samples. This procedure allows us to evaluate the sensitivity of the test setup up to very high frequencies. Should the aperture
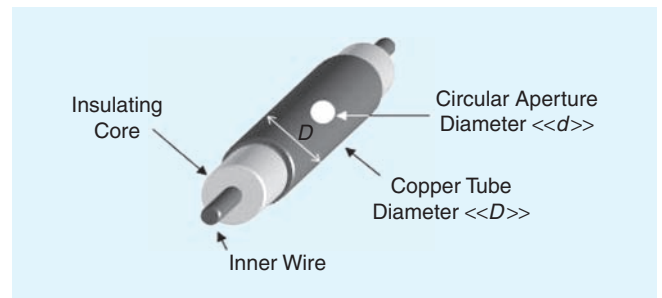

Fig. 12. Calibration sample with small circular aperture: description of the main geometrical parameters.
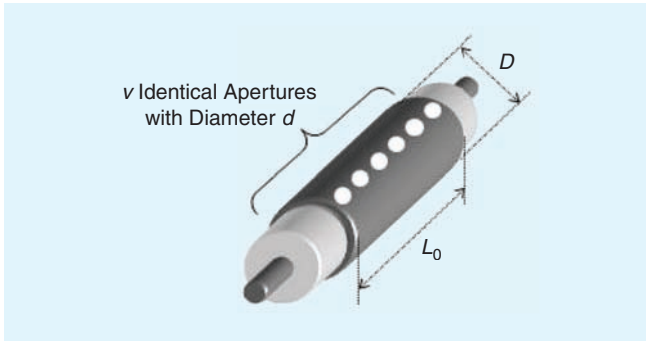
Fig. 13. Calibration sample with v similar uniformly spaced circular apertures.

diameter be comparable or smaller than the shield thickness, the literature provides a correction coefficient for the polarizability computation [7].

In order to appreciate the influence of propagation phenomena on the measurement accuracy, we adopt a sample with a series of regularly-spaced apertures along the generatrix of the copper tube, as illustrated in Fig. 13. The transfer inductance then becomes:

$$L_t = \frac{v}{L_0} \frac{\mu_0 \, \alpha_m}{\pi^2 \, D^2} \qquad (21)$$

where the parameter v indicates the number of identical apertures of diameter d and L_0 is the length of the generatrix along which the holes are uniformly aligned. It should be noted that the transfer inductance of (21) has dimensions of H/m, contrary to the case of a single aperture, for which L_t given by (19) is expressed in H.

Examples of Transfer Impedance Measurements Carried out within 100 MHz to 1 GHz

This Section presents results of measurements conducted on a calibration sample and on coaxial cables with braided shields. The calibration sample is made of a copper tube (diameter D of 10 mm, and thickness of 0.1 mm) with a hole (diameter d of 5 mm). The braided cables are of commercial types KX 15 and KX 4. Comparisons of measurements made on different setups
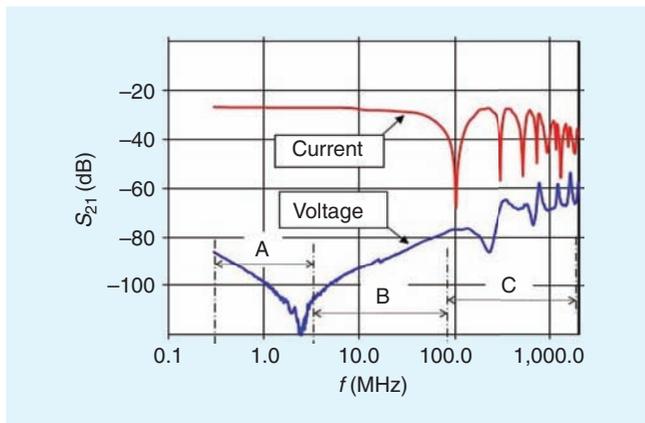

Fig. 14. Test performed on the calibration sample with one small circular aperture. The upper red curve shows the S_{21} vs the frequency when the input of the network analyzer is connected at the current probe. The blue curve below shows S_{21} when the N.A. input is collecting the near end voltage.

(one with shield discontinuity, one of classical triaxial type, and one with wire injection method) are proposed in the following.

Measurements of a Sample with an Aperture

The curves of Fig. 14, referring to a setup with shield discontinuity, show the behaviour of the current measured at the setup input and of the voltage collected at the output, as described in Sect. II. The sample under test is a calibration sample with an aperture.

The results of Fig. 14 are shown between 300 kHz and 2 GHz, but the measurement method is exploitable below 100 MHz, where we observe a reduction of sensitivity due to the reduced dimensions of the sample under test. The vertical scale represents the values of S_{21} (in dB) as given by the network analyzer, of which one port is connected to the input of the measurement bench and the second port is linked either to the current probe installed at the input of the measurement bench or at its output where the sample is short circuited.

The red trace on the upper part of the graph shows the behaviour of S_{21} as obtained with the output port of the network analyzer connected to the current probe. The comparison with Fig. 7 indicates a satisfying agreement with the thin line obtained by simulation of the sample. This condition explains the discrepancies of the positions of maxima and minima of the current. In fact, the first minimum of the experimental curve–actually located at the frequency of 100 MHz–perfectly coincides with the first resonance of the 70-cm long cavity.

The blue trace shows the behaviour of the voltage measured at the end of the sample. The change of this curve with frequency suggests a subdivision of the graph into three separates zones.

Zone **A**, situated between 300 kHz and 30 MHz, is characterized by a monotonic decrease of the curve with frequency: this means that coupling through the sample is dominated by the diffusion of the electric field in the copper thickness of 0.1 mm. Referring to (17), it means that the strength of the second term on the right-hand side, i.e. the transfer reactance, is negligible with respect to the first term. Zone **B**, situated between 30 MHz and 100 MHz, shows a monotonic increase of voltage with frequency: in this case, coupling is clearly dominated by the small aperture and the transfer impedance mainly depends on the second term of (17). In zone **C**, situated between 100 MHz and 2 GHz, the voltage undergoes amplitude fluctuations more and more correlated to propagation phenomena as the frequency grows above 100 MHz. It is ought to be remarked that the resonances evidenced by amplitude maxima are correlated to maxima of the induction current circulating on the sample located in the central part of the cavity.

The transfer impedance above 100 MHz is precisely determined at voltage maxima. The curves of Fig. 15 allow us to compare the transfer impedance measured by means of the discontinuity setup with the straight line derived from (17). It must be noted that–above 100 MHz–the red curve showing the measurement results is obtained by a linear interpolation of transfer impedances determined for each individual voltage resonance. The green curve, limited to the interval 1 MHz–1 GHz, is the result of the transfer reactance calculation, according to (18), (19) and (20): the excellent agreement with the measurement curve is evident.
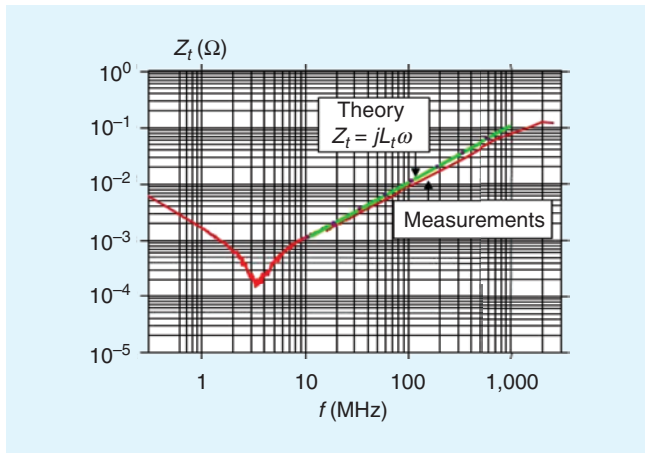
Fig. 15. Transfer impedance of the calibration sample with one aperture deduced from the test carried out with the shield discontinuity method.

Fig. 16. Transfer impedance of the KX15 single braided cable tested successively with the triaxial, wire injection and shield discontinuity methods.

Comparison of Measurements for Three Setups

The objective here is to collect on a single plot (Fig. 16) the curves of the transfer impedances obtained for a classical triaxial setup, the wire injection setup described above in Section II, and the shield discontinuity setup. The triaxial setup was made according to the description of Fig. 4 of our previous paper [1]. The cable used for this comparison is a single braided coaxial one (type KX 15 (RG 58)), and the test length of 10 cm, as already indicated.

The blue line of Fig. 16 represents the transfer impedance obtained by near-end crosstalk voltage measured on a 1-m long cable sample by means of the classical triaxial setup. This curve is undistinguishable from the results of the other methods up to a frequency of approximately 20 MHz. From 20 to 100 MHz, this curve presents significant fluctuations that can be correlated to the de contribution of both propagation phenomena and setup radiation. The physical origin of such discrepancies has been thoroughly discussed in our previous paper [1].

The green line of Fig. 16 represents the transfer impedance obtained by the method of the wire injection. The quasi-monotonic behaviour of this curve up to approximately 1 GHz proves that the technique is well-adapted for the suppression of propagation artefacts. It should be noted that the measurement refers to the far-end crosstalk voltage, but the amplitude fluctuations between 1 and 2 GHz should be related to the setup radiation and to the mismatch of the injection line, both appearing at high frequencies. In fact, we should mention that the evaluation of the perturbation current for the injection-line method is made by taking the ratio of the power injected on the perturbation line, assuming that the value of its input impedance is very close to 50 Ω. However, this impedance is not rigorously invariant, since it depends on the constancy of the characteristic impedance, especially at the transition to the line made of a ribbon conductor glued to the insulation jacket of the cable under test. Also, the section under test is transitioned at its input and output to 50-Ω coaxial cables connected to the UHF source and to the load of the injection line, respectively. Such transitions locally introduce parasitic impedances whose influence can appear in the GHz range.

The red curve is the result of the measurement obtained by means of the shield discontinuity technique. With reference to the plot of Fig. 14, it appears that the impedance curve is known continuously between 300 kHz and 100 MHz, but at
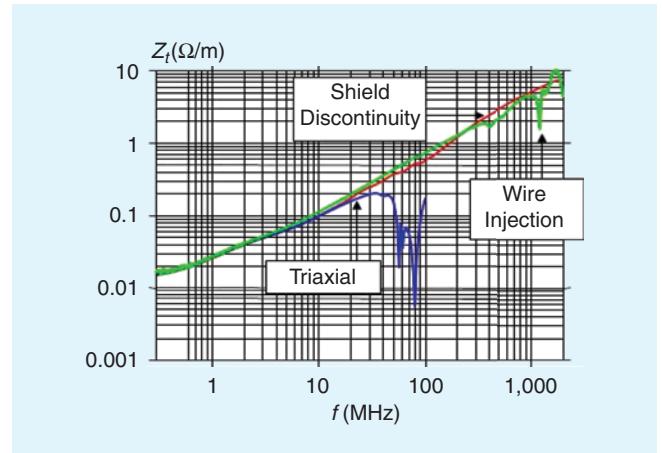
higher frequencies–from 100 MHz and 2 GHz–the value of Z_t is only known for those points where the voltage measured on the test sample presents amplitude maxima. The graph of Fig. 16 confirms that, above 100 MHz, the red curve is a linear interpolation of resonance points.

Braided Shield Behaviour for a Large Frequency Range

In general, transfer impedance of cables with a shield made of a single braid can be modelled by means of the following expression:

$$Z_t = R_0 + j L_t \omega \qquad (22)$$

where the quantity R_0 represents the per-unit-length braid resistance and L_t is the transfer inductance due to magnetic leakage occurring at the junction of the braids composing the carrier conductors. For regular cables, the order of magnitude of these parameters is $R_0 \approx 10$ mΩ/m and $L_t \approx 0.5$ nH/m. However, some cables depart from the model expressed by (22), as in the case of cable type KX 4 (RG 213), whose transfer impedance measured by the shield discontinuity technique is reproduced in Fig. 17.
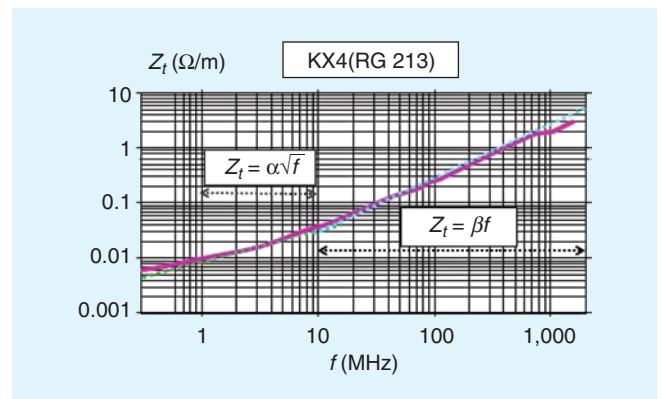

Fig. 17. Typical behaviour of the transfer impedance measured on a single braided cable shield with pitch angle lesser than 45°.

The vertical logarithmic scale of Fig. 17 represents the magnitude of the transfer impedance, and two dotted straight lines are added to the measurement curve (in magenta color). A careful analysis of the graph indicates that, for frequencies between 1 MHz and 10 MHz, the curve agrees with a straight line in logarithmic coordinates, meaning that the transfer impedance is proportional to the square root of frequency. On the contrary, from 10 MHz to 2 GHz, the measured curve is best fitted by a straight line with a slope having a double value of the previous one, meaning a direct proportionality with frequency. Knowing that the shield of RG 213 cables presents a pitch angle smaller than 30°, we can argue that the mechanisms of electromagnetic coupling in this case are rather different from those activated by small apertures, as for the case of the calibration sample reported in Fig. 12. Phase measurements of the transfer impedance show that the transfer impedance model best suited for braids of RG 213 type agrees rather well with the following expression:

$$Z_t = R_0 + k\sqrt{\omega}\, e^{-j\frac{3\pi}{4}} - j\, L_t \omega \qquad (23)$$

where R_0 is the per-unit-length braid resistance, k is a real coefficient depending on the braid parameters and has positive values if the pitch angle with respect to the cable axis is smaller than 45°. In (23), the first two terms are complemented with the transfer impedance of the braid, but–contrary to the model of small apertures described above–the term L_t appears with a negative sign, indicating that the asymptotic phase behaviour tends towards $-\pi/2$ for very high frequencies. These phenomena reveal specific coupling mechanisms described in research work published in previous work about twenty years ago [8], [10].

Conclusion

Although the transfer impedance measurement setups discussed in this paper are specifically designed for the frequency range between 100 MHz and 1 GHz, the measurement principle they implement allows also to explore frequencies below 100 MHz. In fact, the minimum frequency of the measurement bandwidth is set by the HF signal generator and receiver available to the user.

The specificity of setups made for the 100 MHz–1 GHz bandwidth resides in the length reduction (approx 10 cm) of the sample of the shielded cable under test. This means a loss of sensitivity on the order of 20 dB with respect to a classical measurement performed by means of a triaxial setup on a 1-m long cable sample. The sensitivity loss is particularly noticeable for frequencies below 100 MHz, where the transfer impedance of cables for high immunity can be on the order of $\mu\Omega$/m, and in some cases attain even lower values. The consequence is, that for such very good shields, it may be required to compare the measured data obtained by means of the high-frequency setup with the classical tests performed in the triaxial configuration.

It should also be mentioned that measurement setups based on the injection line or on the shield discontinuity, as described in the present paper, are not unique for the frequency bandwidth 100 MHz–1 GHz; different techniques have also been proposed in the literature [9], [11]. However, the injection line and the coaxial discontinuity are likely to be of simpler use.

As far as frequencies above 1 GHz are concerned, it is clear that the devices based on the principle of coupled transmission line reach their validity limits. In fact, as soon as the wavelength approaches the transverse dimension of the metallic tube employed by the shield discontinuity setup, we reach the limit of validity of TEM propagation, and higher order modes appear, and give rise to systematic measurement errors with growing amplitude with frequency. For the injection-line method at frequencies above the GHz, the increase of common-mode current produces additional systematic errors. In both cases, the experience has taught us that the compensation of errors via mathematical or technological tricks is inefficient. Thus, we turned toward the use of shielding effectiveness measurements via electromagnetic field illumination, and we demonstrated that the adoption of mode-stirred reverberation chambers brings interesting insights and allows for the conversion of shielding attenuation measurements into the conventional transfer impedance characteristic.

References

[1] B. Démoulin, L. Koné *Shielded Cable Transfer Impedance Measurements* IEEE-EMC Newsletter, Fall 2010, pp. 30–37.

[2] J. Mueller Cable shielding Test Methods, a Comparison of Different Test Methods EMC 2007, IEEE International Symposium, Honolulu, USA, July 2007, Symp. Record pp 1–6, ISBN 1-4244-1350-8.

[3] L. Martens, A. Madou, B. Vanlandschoot, L. Koné, B. Démoulin, P. Sjöberg, A. Anton, L. Van der Torren, J. Van Koetsem, H. Hoffmann and U. Sthricker *Shielding Of Backplane Interconnection Technology Systems (EU SOBITS project)* IEEE Transactions on EMC, Vol. 42, N°4, November 2000, p 427–440.

[5] R. De Smedt, J. Van Bladen *Magnetic Polarizability of Small Apertures* IEEE Transactions on A.P., Vol. 28, N° 5, September 1980, pp 198–205.

[6] D.A. Hill, M.L. Crawford, M. Kanda, M. Wu *Aperture Coupling to a Coaxial Air Line Theory and Experiment* IEEE Transactions on EMC, Vol. 35, N°1, February 1993, pp 69–74.

[7] J.H. Lee, H.J. Eom *Electrostatic potential through a Circular Aperture in a Thick Conductive Plane* IEEE Transactions on MTT, Vol. 44, N°2, February 1996, pp 341–343.

[8] S. Sali *An Improved Model for the Transfer Impedance Calculation of Braided Coaxial Cables* IEEE Transactions on EMC, Vol. 33, N°2, May 1991, pp 129 –143.

[9] S. Sali *Cable shielding Measurements at Microwave Frequencies* IEE Proceeding, Science Measurement Technology, Vol. 151, N°4, July 2004, pp 235–243

[10] F.M. Tesche, M. Ianoz, T. Karlsson *EMC Analysis Methods and Computational Models* J. Wiley, 1997.

[11] A. Orlandi, G. Antonini, R.M. Rizzi *Equivalent Circuit Model of Cables for Bulk Current Injection (BCI) Test* IEEE Transactions on EMC, Vol. 48, N°4, November 2006, pp 701–713.

Biography

Bernard Démoulin was born in 1946. He received his Ph.D. in 1981 and until 2008, was head of the EMC group at the IEMN-TELICE Laboratory. He is presently professor emeritus at the University of Lille, France. His domain of expertise is mainly related to the effect of electromagnetic coupling through cables, transfer impedance measurement and the study of Mode Stirred Reverberation Chambers. He is a senior member of the French society of electrical engineers (SEE) and an URSI correspondent member.

Lamine Koné was born in 1956; he received his Ph.D. degree in 1989. Since 1990, he has been working as engineer in the IEMN-TELICE laboratory at the University of Lille, France. His domain of expertise deals with EMC measurements, especially concerning the transfer impedance on shielded cables or connectors and tests carried out in mode-stirred reverberation chambers. **EMC**